HHS Public Access

Author manuscript

J Bone Miner Res. Author manuscript; available in PMC 2022 December 01.

Published in final edited form as:

J Bone Miner Res. 2021 December ; 36(12): 2413–2425. doi:10.1002/jbmr.4411.

Notum deletion from late-stage skeletal cells increases cortical bone formation and potentiates skeletal effects of sclerostin inhibition

Roy B. Choi[1], **Whitney A. Bullock**[1], **April M. Hoggatt**[1], **Daniel J. Horan**[1], **Emily Z. Pemberton**[1], **Jung Min Hong**[2], **Xinjun Zhang**[3,4], **Xi He**[3,4], **Alexander G. Robling**[1,5,6,7]

[1]Department of Anatomy, Cell Biology & Physiology, Indiana University School of Medicine, Indianapolis, IN, USA.

[2]Division of Biomedical and Applied Sciences, Indiana University School of Dentistry, Indianapolis, IN, USA.

[3]F. M. Kirby Neurobiology Center, Boston Children's Hospital, Boston, MA, USA.

[4]Department of Neurology, Harvard Medical School, Boston, MA, USA.

[5]Department of Biomedical Engineering, Indiana University–Purdue University at Indianapolis, Indianapolis, IN, USA.

[6]Roudebush VA Medical Center, Indianapolis, IN USA.

[7]Indiana Center for Musculoskeletal Health, Indianapolis, IN, USA.

Abstract

Wnt signaling plays a vital role in the cell biology of skeletal patterning, differentiation, and maintenance. Notum is a secreted member of the α/β-hydrolase superfamily that hydrolyzes the palmitoleoylate modification on Wnt proteins, thereby disrupting Wnt signaling. As a secreted inhibitor of Wnt, Notum presents an attractive molecular target for improving skeletal health. To determine the cell type of action for Notum's effect on the skeleton, we generated mice with Notum deficiency globally ($Notum^{-/-}$) and selectively ($Notum^{f/f}$) in limb bud mesenchyme (Prx1-Cre) and late osteoblasts/osteocytes (Dmp1-Cre). Late-stage deletion induced increased cortical bone properties, similar to global mutants. Notum expression was enhanced in response to sclerostin inhibition, so dual inhibition (Notum/sclerostin) was also investigated using a combined genetic and pharmacologic approach. Co-suppression increased cortical properties beyond either factor alone. Notum suppressed Wnt signaling in cell reporter assays, but surprisingly, also enhanced Shh signaling independent of effects on Wnt. Notum is an osteocyte-active suppressor of

Corresponding author: Alexander G. Robling, Ph.D., Department of Anatomy, Cell Biology & Physiology, Indiana University School of Medicine, 635 Barnhill Dr., MS 5035, Indianapolis, IN 46202, Tel: (317) 274-7489, Fax: (317) 278-2040, arobling@iupui.edu.

Author contributions

RBC, JMH, and AGR generated and validated the mutant mice. RBC, AMH, and WAB conducted Cre/Lox experiments. RBC conducted the antibody studies. DJH conducted the μCT analysis. EZP and RBC conducted the histomorphometry work. RBC conducted mechanical testing, DXA, serum assays. RBC, XZ, and XH conducted cell culture experiments. RBC and AGR wrote the manuscript.

All authors have declared that no conflicts of interest exist.

cortical bone formation that is likely involved in multiple signaling pathways important for bone homeostasis.

INTRODUCTION

The Wnt pathway has emerged as a major regulator of bone cell signaling.[1,2] Genetic mapping of mutations among patients with very high bone mass have revealed numerous genes in the canonical Wnt pathway that contribute significantly to bone mass and strength,[3–5] and consequently present targets for pharmaceutical intervention. Among those targets, the most successfully developed approach to date is the neutralization of Lrp5/6 antagonist sclerostin, via the recently approved biologic EVENITY® (romosozumab-aqqg; Romo). While Romo is efficacious at reducing fracture risk in postmenopausal women at high risk of fracture,[6] other Wnt-based proteins might present equally good targets, either singly or used in combination.[7,8] As our understanding of Wnt biology is constantly expanding and new mechanisms of action for modulation of Wnt are coming to light, it is pertinent to probe those mechanisms for potential utility as therapeutic targets.

One of the more recent proteins identified as a Wnt mediator is the secreted carboxylesterase Notum. Notum was initially thought to function as a glycosylphosphatidylinositol (GPI) anchor lipase, releasing the glypican family of proteoglycans from the membrane via lipase action at their GPI anchor.[9] However, more recent studies have suggested that Notum functions not as a GPI lipase, but rather, as a deacylase that specifically removes the palmitoleic acid modification from serine residues on Wnt proteins.[10,11] In that role, Notum counters the Wnt acylation role of the intracellular MBOAT porcupine,[12] and inhibits Wnt signaling by cleaving a key modification from Wnt that is required for Wnt interaction with its co-receptor Frizzled.[13]

Notum deletion from the genome results in high bone mass specifically in the cortical compartment, with little to no effect in the cancellous compartment.[14] This is a curious but not unexpected finding, as other genes in the Wnt pathway exhibit compartment-specific effects on the skeleton.[15–17] The cellular/molecular mechanisms driving Notum's compartment selectivity are not known, but conceptually they could be harnessed in a therapeutic context to selectively manipulate cortical bone while leaving cancellous bone unperturbed.

In this communication, we generated three lines of Notum loss-of-function mutant mice – global knockouts ($Notum^{-/-}$) and mice harboring conditional alleles ($Notum^{f/f}$) recombined selectively in the limb bud mesenchyme (Prx1-Cre) or late stage osteoblast/osteocyte (Dmp1-Cre). These models permitted investigation of bone-selective effects and the stage of differentiation at which Notum exerts its effects on the skeleton. Further, we sought to investigate the therapeutic potential of Notum in a combination therapy approach (as we have done with inhibition of other Wnt antagonists[7,8]) by investigating whether inactivation of Notum can potentiate the bone-building effects of sclerostin inhibition. Notum might not be selective to Wnt deacylation[18], so we investigated whether Notum modulates another bone-active signaling pathway—hedgehog/Gli—and found that Notum enhances sonic hedgehog-stimulated signaling. Collectively, these results further define a role for

Notum in regulating skeletal properties, and highlight the potential role that Notum might play in synergism with other Wnt mediators and potentially in other pathways such as hedgehog.

RESULTS

Mice with global Notum deletion exhibit significantly increased cortical bone properties.

In order to investigate the skeletal consequences of Notum deletion in mice, we generated Notum global loss-of-function mutants. The last 5 exons of Notum (ex. 8–12) were replaced with a LacZ cassette using a tm1a construct in mouse ES cells, and subsequently crossed to EIIa-Cre (Fig 1A). Genotyping was accomplished using PCR on tail snips (Fig. 1B). Successful targeting was verified by measuring Notum transcript levels and LacZ (knocked into the deleted region) expression in bone and liver tissue extracted from 8-wk old mice. As expected, Notum expression was undetectable both liver and bone from homozygous mutants, whereas LacZ was strongly expressed in the homozygous mutants (Fig. S1A). Body mass was significantly lower in homozygous mutants (KO) compared to WT and heterozygotes, but femur length was not different between WT and KO (Fig. S1B, E). μCT-derived cancellous bone volume in the femur and spine of 17-wk old mice was not increased by Notum deletion (Fig. 1C). Conversely, cortical bone mass was significantly increased at both sites among Notum mutant mice, and was maintained at 30 wks of age in the femur (Fig. S1C). Serial DXA measurements collected from 4–17 wks of age indicated a significant increase in hindlimb BMD (a cortical-rich site) among mutant females but not males (Fig. 1E). Percent fat mass was not different among genotypes but male knockouts became progressively leaner over time (Fig. S1F). The increase in cortical bone mass associated with Notum mutation prompted us to test the femoral diaphyses for changes in mechanical properties, using 3-pt bending tests. Ultimate force and energy to failure were significantly increased in mutants compared to controls, but only for female mice (Fig. 1F). In order to investigate the cellular mechanisms responsible for the increased cortical bone mass, serum from 6-wk mice was collected and assayed for the resorption marker c-terminal telopeptide (CTX). No changes in CTX were detected (Fig. 1G), but significant increases in midshaft femur bone formation rates were found (Fig. 1H and 1I), suggesting a cortical anabolic effect of Notum deletion.

Selective Notum deletion from limb bud mesenchymal cells preferentially increases cortical bone properties.

Previous work indicated that Notum deletion can have body-wide effects unrelated to signaling in bone, including kidney development[19] and metabolic disorders when deleted from the liver.[20] To begin better understanding the role of Notum specifically in limb skeletal cells, we generated loss-of-function floxed mice by crossing the tm1a-targeted mice described above with Rosa26-Flp mice (Fig. 2A), then breeding out Rosa26-Flp and breeding in Prx1-Cre. We evaluated the fidelity of Prx1-Cre-induced recombination of the floxed Notum allele in the limbs vs axial skeleton by performing PCR on genomic DNA extracted from the vertebrae and ulna, using recombination specific primers for Notum. The floxed Notum alleles were recombined in the long bones but not spine when Prx1-Cre was present, and remained unrecombined at all sites in the absence of Cre (Fig. 2B).

DXA-derived BMD in the hind limb was significantly increased in male but not female Cre-positive mice, compared to Cre-negative littermate controls (Fig. 2C). Cre-positive mice exhibited significant increases in cortical bone measurements in the femur but not spine. Cancellous bone volume was not significantly affected in the femur for either sex, but the 5th lumbar vertebra exhibited slightly but significantly greater cancellous bone volume in Cre-positive males. Femoral mechanical properties were significantly increased by Prx1-Cre-induced deletion, and bone formation rates were increased only among males (Fig. 2F). Body mass was unaffected by conditional Notum deletion (Fig. S2).

Selective Notum deletion from late-stage osteoblasts and osteocytes preferentially increases cortical bone properties.

The increases in cortical bone mass phenotype observed in Prx1-Cre/Notum-flox mice largely recapitulated that found in Notum global mutants, suggesting that the cortical effects in the null mice are driven by osteoblast-lineage cells. To further refine the stage of differentiation where Notum might be important for regulating cortical properties, we crossed Notum floxed mice with the late osteoblast/osteocyte driver Dmp1-Cre to induces recombination in very late-stage cells. DXA-derived BMD in the hindlimb was significantly increased in Dmp1-Cre-positive mice, compared to Cre-negative littermates (Fig 3A). Cortical but not cancellous properties of the femur and spine were increased by conditional Notum deletion (Fig. 3B &3C). Femoral mechanical properties were significantly increased by Dmp1-Cre-induced deletion, but bone formation parameters were unaffected (Fig. 3D & 3E). Body mass was unaffected by conditional Notum deletion (Fig. S3).

Notum deletion augments cortical bone gain induced by sclerostin neutralization.

Disabling a Wnt antagonist often induces compensatory upregulation of other Wnt antagonists, a feedback mechanism that maintains normal levels of Wnt signaling (e.g., sclerostin neutralization upregulates Dkk1 expression, and vice versa).[8,21,22] We showed previously using co-inhibition of sclerostin and Dkk1 that this phenomenon can be harnessed for improved anabolic action through multi-targeting.[7] To assess whether there is compensatory upregulation between Sost and Notum, we injected WT mice with a single dose of 25 mg/kg sclerostin antibody (Scl-Ab), sacrificed them 48 hours post-injection, and measured Notum transcripts in the femoral cortex. Notum expression was significantly increased in Scl-Ab-treated mice (but not in Dkk1-Ab-treated mice), compared to vehicle controls (Fig 4A), suggesting that an increase in Notum might be restraining a more robust anabolic effect of sclerostin inhibition. We sought to test this idea by co-injecting mice with a sclerostin inhibitor (Scl-mAb) and a Notum inhibitor (LX5061) to determine whether synergistic anabolic action could be achieved, particularly in cortical bone. However, before combining inhibitors, we tested whether the small molecule inhibitor of Notum, LX5061, induced bone gain on its own, in our hands. LX5061 dose-dependently increased luciferase activity in HEK-TOP cells (which stably express the Wnt/β-catenin reporter Topflash) induced by Wnt3a conditioned media (Fig. 4B), suggesting LX5061 was active. To validate the inhibitor in mice, we designed an *in vivo* experiment where female B6 mice were treated for 6.5 wks with daily subQ injection of 15 mg/kg LX5061. We failed to detect an increase in DXA or μCT properties, with the exception of spine BMD. The experiment was repeated

using a different small molecule Notum inhibitor (ABC99) but again no significant effect on the skeleton was found (data not shown).

As we were not confident that the Notum inhibitor arm of a dual inhibitor study (Notum and sclerostin inhibition) would work, we decided to achieve dual inhibition by combining a genetic and pharmacologic approach, by treating Notum$^{-/-}$ mice with Scl-mAb. We designed a 6-wk Scl-mAb treatment experiment in Notum$^{+/+}$ and Notum$^{-/-}$ mice (Fig. 5A), to test the hypothesis that combining Notum inhibition (deletion) with sclerostin inhibition (neutralizing antibody) might improve cortical bone properties beyond either manipulation alone. Cancellous bone properties were improved by Scl-mAb equally in WT and Notum mutant mice (Fig. 5B & 5C). However, Scl-mAb treatment in mutants increased femur cortical bone mass to a significantly greater extent than in WT controls, suggesting Sost/Notum multitargeting might yield improved cortical bone gain. Similar improvements were found for hindlimb aBMD (Fig. 5D). Bone formation rates and mechanical properties were equally improved by Scl-mAb in mutant and WT mice (Fig. 5E–5G).

Notum modifies both Wnt and Sonic Hedgehog signaling.

In addition to its role in bone homeostasis, Notum was recently identified as a secreted factor that alters adipose tissue metabolism.[23] We looked for an adipose phenotype in Notum$^{-/-}$ mice and identified a reduction in gonadal fat mass among mutants (Fig. S1D). Notum$^{-/-}$ mice had normal triglyceride and free fatty acid levels in the serum (not shown), but serum cholesterol was significantly reduced in the male mutant mice (Fig. 6A). To understand whether Notum directly alters cholesterol levels, we overexpressed WT and mutant (S239) Notum in ECR Shh cells and measured free and total cholesterol in the media. WT Notum increased both free and total cholesterol in the media, but S239 Notum increased only total cholesterol (Fig. 6B). Both expression vectors (WT and S239) were validated in two different Wnt/Topflash cell lines—HEK293 and MLOY4—and performed as expected in response to Wnt (Fig. 6C). Given the observed effect of Notum on cholesterol liberation, we next looked at whether Notum might mediate bone-active ligands that exhibit cholesterol modifications, including Sonic Hedgehog (Shh). Light II cells (NIH3T3 fibroblast line stably transfected with a Gli1-driven luciferase reporter) were treated with Shh conditioned media (Shh CM) after transfection with Notum WT or S293 plasmids, or co-treatment with recombinant mouse Notum (mNTM; Fig. 6D & 6E). In both cases, increased Notum levels enhanced Shh signaling, a result we confirmed in the osteocyte-like line IDGSW3 using *Gli1* expression (Fig. 6F). Conceivably, the effect of Notum on Shh signaling could be driven by Notum action on Wnt, where changes in inactivated Wnt (induced by Notum-mediated deacylation) trigger changes in Shh expression/signaling. To address a potential Wnt feedback loop, we repeated the Shh CM treated Light II cell experiments in cultures pretreated with the porcupine inhibitor LGK974 (Fig 6G) or co-treated with several recombinant Wnts (Fig. 6H). Neither a reduction (LGK974) or increase (Wnt 1, 3a, 10b, 16) in Wnt signaling altered the Light II signal, suggesting that Notum's effects on Shh signaling are not explained by Notum-mediated deacylation of Wnt. Finally, to further investigate Notum effects on Shh signaling, we transfected Shh producing cells with WT or mutant Notum plasmids, precipitated the proteins separately from the media and whole cell lysate, and probed for Shh by immunoblot. Secreted and whole cell fractions

exhibited a reduction in the N-terminal fragment of Shh (Shh-Np) when WT and mutant Notum were expressed. (Fig. 6I).

DISCUSSION

Our main goal in this study was to characterize the effect of Notum inhibition at different stages of skeletal cell differentiation, and to evaluate its role as a modifier of sclerostin neutralization activity in cortical bone. Mice with global Notum loss-of-function mutations have been reported previously to exhibit a high bone mass phenotype in the cortical compartment,[14] a result we were able to confirm with our model. It is interesting that another group[24] reported the creation of a Notum global mutant mouse which could not be studied as a homozygous mutant because 90% of the pups were stillborn, and those that survived were unhealthy and did not reach 9 wks of age. We too had survival/growth issues with our homozygous mutant model when on a pure B6 background (data not shown), but once we put them on to a 50/50 mixed background of B6/129, the knockouts had a normal birth ratio and survived normally. A Notum floxed model that underwent induced global deletion later in life using Cag-CreER, and also in the osteoblast population using Runx2-Cre, both yielded a cortical phenotype.[24]

Notum was recently identified as one of the 20 most highly expressed genes in the osteocyte[25], which prompted us to investigate whether the osteocyte is the cell type of action for Notum's effects on cortical bone. To accomplish this, we generated mice with both early- (Prx1-Cre-mediated) and late-stage (Dmp1-Cre-mediated) deletion of Notum in the MSC/osteoblast/osteocyte lineage, using a floxed model. Both Prx1- and Dmp1-driven deletion of Notum induced a high cortical bone mass phenotype in the mice. Given that deletion induced by Prx1-Cre is maintained in all cells downstream in the differentiation lineage (including osteocytes), those experiments suggest that late-stage deletion is driving the skeletal phenotype. One consistent observation among our models and the other published models is a lack of cancellous bone phenotype when Notum is mutated or when small-molecule/biologic inhibitors are administered to mice.[14,26] The reasons for the selective cortical effects in bone are unclear, as the few Notum expression studies in bone that have been completed make no comparison between cortical and cancellous expression/activity; that level of analysis would be exceptionally difficult in mice.

Gene expression studies in Scl-Ab treated mice revealed an upregulation of Notum transcripts in cortical bone, suggesting the potential existence of a negative feedback loop that restrains the anabolic effects of sclerostin inhibition. We had intended to conduct a dual-inhibitor study in WT mice, simultaneously targeting sclerostin and Notum with injectable inhibitors in genetically normal mice. The advantage of that design is that (1) the skeletal cells in all mice are naïve, that is, there is no physiologic accommodation to lifelong absence of targeted protein, and (2) the combined effects of dual inhibition can be compared to individual treatments to determine the level of potentiation. The efficacy of sclerostin antibody has been validated numerous times in our lab,[27–30] but when we tested the efficacy the Notum inhibitor LX5061 in initial experiments, we were unable to detect a significant increase in cortical properties (though a nonsignificant trend was noted). It is unclear why those LX5061 experiments did not work, but it is possible that our route of

administration (daily subQ) was flawed, as previous successful studies reported either oral gavage or food supplementation.[14] To investigate co-inhibition of sclerostin and Notum, we decided to administer sclerostin antibody to Notum$^{-/-}$ mice. This approach had the advantage of neutralizing all Notum. In those studies, we were able to detect a significant improvement in some, but not all, cortical parameters and DXA-based endpoints.

Notum was recently redefined in terms of its enzymatic activity. For many years it was thought to function as a GPI anchor lipase, releasing membrane-bound glypicans into the extracellular environment.[9,31] However, more recent studies failed to confirm a role for Notum in GPI-mediated glypican release, but its role as a potent Wnt deacylase was introduced[10,11] and confirmed by subsequent work.[32,33] Additional enzymatic roles for Notum (e.g., as a ghrelin deacylase) are coming to light.[18] Our cholesterol measurements in mutant mouse serum and transfected cell culture supernatants prompted us to look at whether other bone-active pathways meditated by lipid-modified proteins are altered by Notum. The hedgehog (HH) signaling pathway is one such pathway, and it is a key regulator of osteochondral development and mesenchymal homeostasis in adult tissues.[34,35] HH ligands (Sonic, Indian, Desert) activate the Gli family of transcription factors by initially binding and inhibiting the Patched (Ptc) receptor, which normally (in the “off state”) induces sonic suppression/degradation of the GCPR Smoothened (Smo).[36] Hedgehog-stimulated Ptc receptors derepress Smo, which activates a cascade of cytosolic events that ultimately results in increased nuclear translocation of Gli. Previous work suggested that Notum does not affect HH signaling because hypomorphic alleles of Notum introduced into *Drosophila* do not impair HH signaling.[37,38] However, we found that overexpression of Notum or addition of recombinant Notum enhanced HH reporter activity and/or Gli1 expression in bone cells and HEK cells. Notum increased free cholesterol in the media of Shh producing cell cultures but not in media from control cultures, suggesting that membrane cholesterol was not the source. As cholesterol can directly activate Smo and the downstream HH pathway,[39–42] it is possible that Notum releases the cholesterol modification of Shh, which is both cholesterylated and S-palmitoylated.[43]

Our study has several limitations. First, the global Notum mutants were significantly lighter than their WT littermates. This made DXA and μCT interpretation more complicated that among groups of the same body size/weight. Others have addressed this issue using a global deletion of floxed alleles using an inducible Cre driver.[24] We were able to overcome this issue using the floxed model with both Dmp1-Cre and Prx1-Cre, which presented no body mass differences related to Cre. Second, we were not able to conduct the dual inhibition study on the same genetic background. Failure to find a significant skeletal effect of the small molecule Notum inhibitor precluded using the reagent in a dual inhibitor study, but it could the case that the compound would have interaction when given with Scl-Ab. We found a similar scenario with Dkk1, where administration of Dkk1 antibody alone showed no consistent anabolic effects in mice, but combining it with Scl-Ab enhanced the latter’s effects by several fold.[7]

In summary, the secreted lipase Notum has significant inhibitory effects on the cortical compartment of the mouse skeleton. Notum appears to be important at the osteocyte stage in terms of exerting its effects on bone anabolism. The bone building effects of

sclerostin neutralization are potentiated by Notum deletion, suggesting a new avenue to improve cortical and cancellous bone, with particular improvement in cortical bone. Notum modulates hedgehog signaling activity, independent of any effects on Wnt deacylation. Further exploration of Notum targeting as a treatment for bone disorders will likely have significant impact on our understanding of basic bone cell biology and therapeutic options for the clinic.

MATERIALS AND METHODS

Generation of genetically modified mice

Notum deletion in mice was conducted by purchasing Notum tm1a-targeted embryonic stem (ES) cells from EUCOMM, which were expanded and injected into blastocysts, returned to pseudopregnant females, and screened for germline transmission in pups. Briefly, the correctly targeted mice harbor *LacZ* and *Neo* cassettes in intron 7, which are flanked by frt sequence. The Neo cassette is separately flanked by loxP, and a third loxP was introduced after exon 12. To generate global knockout mice (and a functional in-frame *lacZ* knockin allele), the tm1a targeted mice were crossed to EIIa-Cre mice described previously (Jax stock 003724) which express Cre in the early oocyte and induce germline recombination of loxP.[44] Conversely, to convert the tm1a allele to a tm1c conditional floxed allele, Notum tm1a mice were crossed to Rosa26-Flp mice (Jax stock 012930; described elsewhere[45]) to induce germline recombination of the frt sites and delete the *LacZ*/*Neo*/5'loxP insert, leaving exons 8–12 flanked by loxP. These tm1c mice were then crossed to the Prx1-Cre (Jax stock 005584) or Dmp1-Cre (Jax stock 023047) to induce conditional deletion of Notum exons 8–12 in limb bud mesenchyme (Prx1) or late-stage osteoblasts/osteocytes (Dmp1). Both Cre models have been described elsewhere.[46,47] All mouse lines were validated by PCR. Notum global mutants were on a mixed background of B6 and 129/SvJ, whereas floxed mice and Prx1/Dmp1 Cre drivers were on a pure C57BL/6J background. Mice were housed 3–5 per cage in 12 hr light/dark conditions, and were fed Teklad Global Diet (2018SX) ad libitum.

Study approval

All animal procedures were performed in accordance with relevant federal guidelines and conformed to the Guide for the Care and use of Laboratory Animals (8th Edition).[48] The animal facility at Indiana University is an AAALAC-accredited facility and all mouse procedures were performed in accordance with the IACUC guidelines and approvals.

Dual-energy x-ray absorptiometry (DXA)

Collection of repeated DXA measurements on live mice are described and validated elsewhere.[27] Briefly, isoflurane anesthetized mice were scanned on a PIXImus II (GE Lunar) densitometer at 4, 6, 9, 12, and 17 weeks of age for *Notum* global, floxed Prx1-Cre and Dmp1-Cre mice. For the antibody (Scl-mAb) studies, mice were scanned at the beginning of treatment (9 wks) and again at the terminal timepoint (16 wks). Bone mineral density (BMD) was measured for the whole body, lumbar spine (L3–L5), and right hindlimb using the Lunar ROI (Region of Interest) tools.

Microcomputed tomography (μCT)

Formalin-fixed femora and 5th lumbar vertebrae (L5) were scanned, reconstructed, and analyzed on a Scanco μCT-35 as previously described[27] using 10-μm resolution, 50-kV peak tube potential and 151-ms integration time. Standard parameters related to cancellous and cortical bone architecture were measured.[49]

Histological analysis

All the mice were given various combinations of demeclocycline (40 mg/kg), oxytetracycline HCl (80 mg/kg), calcein (12 mg/kg) and alizarin complexone (20 mg/kg) via subcutaneous/intraperitoneal injection (S.C.,I.P.) to label mineralizing bone, at the time points indicated for each experiment (see figure legends). After sacrifice at indicated time points, the femurs were fixed, dehydrated, processed for plastic-embedded histomorphometry and cut at midshaft for histological evaluation as previously described.[7] Briefly, periosteal and endocortical bone formation parameters, including mineralizing surface (MS/BS; %), mineral apposition rate (MAR; μm/d), and bone formation rate (BFR/BS; $\mu m^3/\mu m^2/yr$), were calculated using standard protocols.[50]

Biomechanical testing

Parameters related to whole bone strength were measured using 3-point bending tests as previously described.[7] Briefly, each fresh-frozen femur was thawed and loaded to failure in monotonic compression, during which force and displacement were collected every 0.01 seconds. From the ultimate force, energy to failure and post-yield displacement were calculated using standard equations.[51]

Serum C-terminal telopeptide (CTX) measurement

Serum concentration of the resorption marker CTX was measured by a commercially available ELISA (RatLaps; IDS Inc.) as previously described.[52] Briefly, blood samples were collected from overnight fasted 6 week-old mice at the retromandibular vein. Blood samples were permitted to clot at room temperature for 30 minutes, spun at 5,000 g to separate the serum, and frozen at −80°C. Thawed serum samples were assayed for CTX in triplicate according to the manufacturer's instructions.

RNA isolation and quantitative polymerase chain reaction (qPCR)

Snap-frozen femur, tibia diaphysis and liver from each mice (see figure legends) were pulverized in liquid N_2 and processed for total RNA isolation as previously described.[52] Briefly, total RNA was isolated from the femur/tibia diaphyses (isolated cortical tubes with periosteum and marrow removed) and liver using previously described cryo-pulverization and Qiagen RNeasy kits. cDNAs were reverse transcribed using high-capacity cDNA reverse transcription kits (Applied Biosystems, Inc.). Quantitative PCR was performed on an ABI Quantstudio Flex 7 (Applied Biosystems, Inc.) using FastStart Universal Probe Master ROX mix (Roche). *Notum* and *LacZ* expression were calculated using the 2- ΔCt method and normalized to transcripts for the housekeeper 60S acidic ribosomal protein P2 (*RPLP2*) for bone and glyceraldehyde-3-phosphate dehydrogenase (*GAPDH*) for liver (see Table1 for primer information).

Cell culture, transfection and reporter assays

Wnt producing and reporting cell lines—*HEK-293-Topflash, MLO-Y4-Topflash, L-Wnt3a* cell lines were cultured and maintained as described elsewhere.[53–55] Briefly, HEK cells were maintained in Dulbecco's modified Eagle's medium (DMEM; Invitrogen) supplemented with 10% fetal bovine serum (FBS) with 0.4mg/ml of G418. MLOY4 cells were cultured in α-Minimum Eagle's Medium(α-MEM) supplemented with 2.5% calf serum(CS), FBS and 1% penicillin-streptomycin (Invitrogen). L- or L-Wnt3a conditioned media were generated by diluting highly concentrated media from L mouse fibroblasts (L-cells) or stably transfected Wnt3a L-cells (L-Wnt3a) in serum free media. After collecting supernatant, cell debris was removed by centrifugation and the clarified fraction was stored at −80°C. Topflash cells (7X Tcf/Lef1 binding sites, driving a luciferase reporter) were plated in 24-well plates and grown overnight. The following day, the cultures were incubated with L- (control) or L-Wnt3a-conditioned medium for 24 hours. The strength of the Wnt/β-catenin signal was measured using the Bio-Glo luciferase assay kit (Luciferase Assay System, Promega (Madison, WI) according to manufacturer's protocols.

Shh light II culture and reporter assay—Shh light II and ECR Shh HEK293 cells, described previously,[56,57] were purchased from Johns Hopkins University and maintained according to the cell bank's protocols. Briefly, cells were maintained in Dulbecco's modified Eagle's medium (DMEM; Invitrogen) supplemented with 10% fetal bovine serum (FBS) with 0.4mg/ml of G418 and zeocin (Invitrogen). Shh conditioned medium was generated by diluting highly concentrated ECR Shh HEK293 medium with serum free media. After collecting supernatant, cell debris was removed by centrifugation and the clarified fraction was stored at −80°C. Shh-Light II cells were plated in 24-well plates and grown overnight. The following day, the cultures were incubated with Shh conditioned medium or medium from control HEK cultures, for 24 hours. The strength of the Shh/Gli signal was measured using the Dual-Glo luciferase assay (Luciferase Assay System, Promega (Madison, WI) according to manufacturer's protocols.

Cholesterol measurement assay—ECR Shh cells were grown to 70% confluence in 60 or 100 mm dishes. 24 hrs later, the cells were transfected with plasmids containing empty vector (EV), Notum wild-type (NTM WT) or mutant Notum (NTM S239) for 48 hrs. After 48hrs, cell supernatants were collected and debris was cleared by centrifugation at 5000g for 15 min followed by filtration using a 0.22μm filter. Total and free cholesterol concentration were measured in triplicate using a commercially available cholesterol plate assay (Cholesterol/Cholesterol Ester-Glo assay J3190, Promega) according to the manufacturer's instructions.

IDG-SW3 culture—IDG-SW3 cells were kindly provided by Dr. Lynda Bonewald (Indiana University School of Medicine). Cells were maintained as previously described.[58]

Plasmids and reagents

Plasmids (*Notum wild-type and Notum S239A mutant*) are described elsewhere.[11] Cells were seeded at 70% confluence in 6-well plates and transfected with plasmids (Empty vector, NTM WT and NTM S239A) (2μg) using either Lipofectamine 2000 (Invitrogen) or

Mirus TransIT-LT1 (Mirus) for 48 hours and transferred to 24-well plates for further assay. Mouse recombinant Notum protein was synthesized and provided by Indiana Biomedical Research Institute (IBRI).

Immunobloting

For whole cell lysates, proteins were harvested from PBS-washed cells using mild lysis buffer (150mM sodium chloride, 1% NP-40, 50mM Tris pH 8.0) supplemented with protease inhibitor cocktail (Sigma-Aldrich, Inc.). Proteins from supernatants were collected using cold-acetone precipitation followed by centrifugation at 14,000g for 10 min. Both mixtures were incubated on ice for 15 min and centrifuged at 16,000g for 15 min. Supernatant and whole cell lysate protein concentrations were calculated by the BCA method. 25μg of protein extracts were run on SDS-PAGE gels, transferred to nitrocellulose and incubated with following antibodies diluted at 1:500–1000 ratio in 5% BSA solution: anti-FLAG (DYKDDDDK (FG4R)-MA1-91878, Thermo fisher), anti-Shh-N (AF464,R&D), anti-β-actin (Sigma A3854). Blots were incubated with secondary antibody-conjugated HRP and developed with ECL western blotting detection reagents as described elsewhere.[59] Probed membranes were stripped with Reblot strong stripping solution (Millipore) for 15mins, washed, re-blocking with 5% skim milk, then reprobed with anti-β-actin for normalization. For supernatant normalization, membranes were ponceau S stained before blocking.

Statistical analysis

Statistical analyses were performed by using JMP (version 4.0, SAS Institute Inc.). The radiographic, histomorphometric, and biomechanical endpoints were analyzed using either student t-test or ANOVA followed by Tukey's-HSD test for posthoc comparisons. Time series data were analyzed with repeated-measures ANOVA. All Graphs were depicted in Whisker-boxplots with interquartile range. The median value is denoted as a line within the box. Statistical significance was indicated in actual p value in each graph.

Supplementary Material

Refer to Web version on PubMed Central for supplementary material.

Acknowledgments

Financial support was provided by the NIH (AR053237 to AGR; AG069489 to RBC), the US Department of Veterans Affairs (BX001478 to AGR). Sclerostin antibody was provided by Amgen Inc. (Thousand Oaks, CA) and UCB (Brussels, Belgium). LX5061 was synthesized and kindly provided by Drs. Linda Ma and Jeffrey Dodge at Eli Lilly, Inc. The MLOY4-Topflash cell line was kindly provided by Drs. Nuria Lara-Castillo and Mark L. Johnson (University of Missouri-Kansas City, School of Dentistry). The content is solely the responsibility of the authors and does not necessarily represent the official views of the NIH. The funders had no role in study design, data collection and analysis, decision to publish, or preparation of the manuscript.

References

1. Baron R & Kneissel M (2013) WNT signaling in bone homeostasis and disease: from human mutations to treatments. Nat Med 19(2):179–192 [PubMed: 23389618]
2. Nusse R (2005) Wnt signaling in disease and in development. Cell Res 15(1):28–32 [PubMed: 15686623]

3. Balemans W, Ebeling M, Patel N, Van Hul E, Olson P, Dioszegi M,… Van Hul W (2001) Increased bone density in sclerosteosis is due to the deficiency of a novel secreted protein (SOST). Hum Mol Genet 10(5):537–543 [PubMed: 11181578]
4. Little RD, Carulli JP, Del Mastro RG, Dupuis J, Osborne M, Folz C,… Johnson ML (2002) A mutation in the LDL receptor-related protein 5 gene results in the autosomal dominant high-bone-mass trait. Am J Hum Genet 70(1):11–19. [PubMed: 11741193]
5. Leupin O, Piters E, Halleux C, Hu S, Kramer I, Morvan F,… Kneissel M (2011) Bone overgrowth-associated mutations in the LRP4 gene impair sclerostin facilitator function. J Biol Chem 286(22):19489–19500. [PubMed: 21471202]
6. Slomski A (2017) Romosozumab Prevents Fractures in Women With Osteoporosis. JAMA 318(20):1968
7. Witcher PC, Miner SE, Horan DJ, Bullock WA, Lim KE, Kang KS,… Robling AG (2018) Sclerostin neutralization unleashes the osteoanabolic effects of Dkk1 inhibition. JCI Insight 3(11).
8. Florio M, Gunasekaran K, Stolina M, Li X, Liu L, Tipton B,… Ominsky MS (2016) A bispecific antibody targeting sclerostin and DKK-1 promotes bone mass accrual and fracture repair. Nat Commun 7:11505. [PubMed: 27230681]
9. Traister A, Shi W & Filmus J (2008) Mammalian Notum induces the release of glypicans and other GPI-anchored proteins from the cell surface. Biochem J 410(3):503–511 [PubMed: 17967162]
10. Kakugawa S, Langton PF, Zebisch M, Howell SA, Chang TH, Liu Y,… Vincent JP (2015) Notum deacylates Wnt proteins to suppress signalling activity. Nature 519(7542):187–+ [PubMed: 25731175]
11. Zhang XJ, Cheong SM, Amado NG, Reis AH, MacDonald BT, Zebisch M,… He X (2015) Notum Is Required for Neural and Head Induction via Wnt Deacylation, Oxidation, and Inactivation. Dev Cell 32(6):719–730 [PubMed: 25771893]
12. Chang SC & Magee AI (2009) Acyltransferases for secreted signalling proteins (Review). Mol Membr Biol 26(1):104–113 [PubMed: 19169935]
13. Janda CY, Waghray D, Levin AM, Thomas C & Garcia KC (2012) Structural basis of Wnt recognition by Frizzled. Science 337(6090):59–64. [PubMed: 22653731]
14. Brommage R, Liu J, Vogel P, Mseeh F, Thompson AY, Potter DG,… Liu Q (2019) NOTUM inhibition increases endocortical bone formation and bone strength. Bone Res 7:2. [PubMed: 30622831]
15. Kiper POS, Saito H, Gori F, Unger S, Hesse E, Yamana K,… Baron R (2016) Cortical-Bone Fragility--Insights from sFRP4 Deficiency in Pyle's Disease. N Engl J Med 374(26):2553–2562. [PubMed: 27355534]
16. Zheng HF, Tobias JH, Duncan E, Evans DM, Eriksson J, Paternoster L,… Lorentzon M (2012) WNT16 influences bone mineral density, cortical bone thickness, bone strength, and osteoporotic fracture risk. PLoS Genet 8(7):e1002745. other authors have declared that no competing interests exist. [PubMed: 22792071]
17. Bennett CN, Longo KA, Wright WS, Suva LJ, Lane TF, Hankenson KD & MacDougald OA (2005) Regulation of osteoblastogenesis and bone mass by Wnt10b. Proc Natl Acad Sci U S A 102(9):3324–3329. [PubMed: 15728361]
18. Zhao Y, Schuhmacher LN, Roberts M, Kakugawa S, Bineva-Todd G, Howell S,… Jones EY (2021) Notum deacylates octanoylated ghrelin. Mol Metab:101201 [PubMed: 33647468]
19. Vogel P, Read RW, Hansen GM, Powell DR, Kantaputra PN, Zambrowicz B & Brommage R (2016) Dentin Dysplasia in Notum Knockout Mice. Vet Pathol 53(4):853–862 [PubMed: 26926082]
20. Canal F, Charawi S, Grimber G, Houbron C, Drouet V, Colnot S,… Perret C (2016) Generation of Mice with Hepatocyte-Specific Conditional Deletion of Notum. PLoS One 11(3):e0150997. [PubMed: 26974334]
21. van Lierop AH, Moester MJ, Hamdy NA & Papapoulos SE (2014) Serum Dickkopf 1 levels in sclerostin deficiency. J Clin Endocrinol Metab 99(2):E252–256 [PubMed: 24302746]
22. Stolina M, Dwyer D, Niu QT, Villasenor KS, Kurimoto P, Grisanti M,… Kostenuik PJ (2014) Temporal changes in systemic and local expression of bone turnover markers during six months of sclerostin antibody administration to ovariectomized rats. Bone 67:305–313 [PubMed: 25093263]

23. Seldin MM, Koplev S, Rajbhandari P, Vergnes L, Rosenberg GM, Meng Y,… Lusis AJ (2018) A Strategy for Discovery of Endocrine Interactions with Application to Whole-Body Metabolism. Cell Metab 27(5):1138–1155 e1136. [PubMed: 29719227]
24. Moverare-Skrtic S, Nilsson KH, Henning P, Funck-Brentano T, Nethander M, Rivadeneira F,… Ohlsson C (2019) Osteoblast-derived NOTUM reduces cortical bone mass in mice and the NOTUM locus is associated with bone mineral density in humans. FASEB J 33(10):11163–11179. [PubMed: 31307226]
25. Youlten SE, Kemp J, Logan JG, Ghirardello EJ, Sergio C, Dack MRG,… Croucher P (2020) Osteocyte transcriptome mapping identifies a molecular landscape controlling skeletal homeostasis and susceptibility to skeletal disease. bioRxiv
26. Tarver JE Jr., Pabba PK, Barbosa J, Han Q, Gardyan MW, Brommage R,… Carson KG (2016) Stimulation of cortical bone formation with thienopyrimidine based inhibitors of Notum Pectinacetylesterase. Bioorg Med Chem Lett 26(6):1525–1528 [PubMed: 26897593]
27. Kedlaya R, Veera S, Horan DJ, Moss RE, Ayturk UM, Jacobsen CM,… Robling AG (2013) Sclerostin inhibition reverses skeletal fragility in an Lrp5-deficient mouse model of OPPG syndrome. Sci Transl Med 5(211):211ra158.
28. Lim KE, Bullock WA, Horan DJ, Williams BO, Warman ML & Robling AG (2021) Co-deletion of Lrp5 and Lrp6 in the skeleton severely diminishes bone gain from sclerostin antibody administration. Bone 143:115708. [PubMed: 33164872]
29. Lewis KJ, Choi RB, Pemberton EZ, Bullock WA, Firulli AB & Robling AG (2019) Twist1 Inactivation in Dmp1-Expressing Cells Increases Bone Mass but Does Not Affect the Anabolic Response to Sclerostin Neutralization. Int J Mol Sci 20(18).
30. Bullock WA, Hoggatt AM, Horan DJ, Elmendorf AJ, Sato AY, Bellido T,… Robling AG (2019) Lrp4 Mediates Bone Homeostasis and Mechanotransduction through Interaction with Sclerostin In Vivo. iScience 20:205–215. [PubMed: 31585407]
31. Filmus J, Capurro M & Rast J (2008) Glypicans. Genome Biol 9(5):224. [PubMed: 18505598]
32. Atkinson BN, Steadman D, Zhao Y, Sipthorp J, Vecchia L, Ruza RR,… Fish PV (2019) Discovery of 2-phenoxyacetamides as inhibitors of the Wnt-depalmitoleating enzyme NOTUM from an X-ray fragment screen. Medchemcomm 10(8):1361–1369. [PubMed: 31534655]
33. Fang Y & Que J (2018) Notum balances Wnt signaling during tracheal cartilage development. Dev Biol 437(2):61–62 [PubMed: 29476723]
34. Beachy PA, Karhadkar SS & Berman DM (2004) Tissue repair and stem cell renewal in carcinogenesis. Nature 432(7015):324–331 [PubMed: 15549094]
35. Yang J, Andre P, Ye L & Yang YZ (2015) The Hedgehog signalling pathway in bone formation. Int J Oral Sci 7(2):73–79. [PubMed: 26023726]
36. Falkenstein KN & Vokes SA (2014) Transcriptional regulation of graded Hedgehog signaling. Semin Cell Dev Biol 33:73–80. [PubMed: 24862856]
37. Kakugawa S, Langton PF, Zebisch M, Howell S, Chang TH, Liu Y,… Vincent JP (2015) Notum deacylates Wnt proteins to suppress signalling activity. Nature 519(7542):187–192. [PubMed: 25731175]
38. Ingham PW, Nakano Y & Seger C (2011) Mechanisms and functions of Hedgehog signalling across the metazoa. Nat Rev Genet 12(6):393–406 [PubMed: 21502959]
39. Kinnebrew M, Iverson EJ, Patel BB, Pusapati GV, Kong JH, Johnson KA,… Rohatgi R (2019) Cholesterol accessibility at the ciliary membrane controls hedgehog signaling. Elife 8.
40. Luchetti G, Sircar R, Kong JH, Nachtergaele S, Sagner A, Byrne EF,… Rohatgi R (2016) Cholesterol activates the G-protein coupled receptor Smoothened to promote Hedgehog signaling. Elife 5.
41. Deshpande I, Liang J, Hedeen D, Roberts KJ, Zhang Y, Ha B,… Manglik A (2019) Smoothened stimulation by membrane sterols drives Hedgehog pathway activity. Nature 571(7764):284–288. [PubMed: 31263273]
42. Huang P, Nedelcu D, Watanabe M, Jao C, Kim Y, Liu J & Salic A (2016) Cellular Cholesterol Directly Activates Smoothened in Hedgehog Signaling. Cell 166(5):1176–1187 e1114. [PubMed: 27545348]

43. Buglino JA & Resh MD (2008) Hhat is a palmitoylacyltransferase with specificity for N-palmitoylation of Sonic Hedgehog. J Biol Chem 283(32):22076–22088. [PubMed: 18534984]
44. Lakso M, Pichel JG, Gorman JR, Sauer B, Okamoto Y, Lee E,… Westphal H (1996) Efficient in vivo manipulation of mouse genomic sequences at the zygote stage. Proc Natl Acad Sci U S A 93(12):5860–5865. [PubMed: 8650183]
45. Raymond CS & Soriano P (2007) High-efficiency FLP and PhiC31 site-specific recombination in mammalian cells. PLoS One 2(1):e162. [PubMed: 17225864]
46. Logan M, Martin JF, Nagy A, Lobe C, Olson EN & Tabin CJ (2002) Expression of Cre Recombinase in the developing mouse limb bud driven by a Prxl enhancer. Genesis 33(2):77–80 [PubMed: 12112875]
47. Lu Y, Xie Y, Zhang S, Dusevich V, Bonewald LF & Feng JQ (2007) DMP1-targeted Cre expression in odontoblasts and osteocytes. J Dent Res 86(4):320–325 [PubMed: 17384025]
48. Board NA (2011) Guide for the care and use of laboratory animals (National Academy of Sciences, USA) 8 Ed.
49. Bouxsein ML, Boyd SK, Christiansen BA, Guldberg RE, Jepsen KJ & Muller R (2010) Guidelines for assessment of bone microstructure in rodents using micro-computed tomography. J Bone Miner Res 25(7):1468–1486 [PubMed: 20533309]
50. Dempster DW, Compston JE, Drezner MK, Glorieux FH, Kanis JA, Malluche H,… Parfitt AM (2013) Standardized Nomenclature, Symbols, and Units for Bone Histomorphometry: A 2012 Update of the Report of the ASBMR Histomorphometry Nomenclature Committee. Journal of Bone and Mineral Research 28(1):1–16 [PubMed: 23255454]
51. Turner CH & Burr DB (1993) Basic biomechanical measurements of bone: a tutorial. Bone 14(4):595–608 [PubMed: 8274302]
52. Robling AG, Kedlaya R, Ellis SN, Childress PJ, Bidwell JP, Bellido T & Turner CH (2011) Anabolic and Catabolic Regimens of Human Parathyroid Hormone 1–34 Elicit Bone- and Envelope-Specific Attenuation of Skeletal Effects in Sost-Deficient Mice. Endocrinology 152(8):2963–2975 [PubMed: 21652726]
53. Xu Q, Wang Y, Dabdoub A, Smallwood PM, Williams J, Woods C,… Nathans J (2004) Vascular development in the retina and inner ear: control by Norrin and Frizzled-4, a high-affinity ligand-receptor pair. Cell 116(6):883–895 [PubMed: 15035989]
54. Willert K, Brown JD, Danenberg E, Duncan AW, Weissman IL, Reya T,… Nusse R (2003) Wnt proteins are lipid-modified and can act as stem cell growth factors. Nature 423(6938):448–452 [PubMed: 12717451]
55. Lara N & Johnson ML (2017) Development and characterization of stably transfected TOPFlash MLO-Y4 cell lines. J Bone Miner Res 32 32(Suppl. 1):0197
56. Taipale J, Chen JK, Cooper MK, Wang B, Mann RK, Milenkovic L,… Beachy PA (2000) Effects of oncogenic mutations in Smoothened and Patched can be reversed by cyclopamine. Nature 406(6799):1005–1009 [PubMed: 10984056]
57. Chen JK, Taipale J, Young KE, Maiti T & Beachy PA (2002) Small molecule modulation of Smoothened activity. Proc Natl Acad Sci U S A 99(22):14071–14076. [PubMed: 12391318]
58. Woo SM, Rosser J, Dusevich V, Kalajzic I & Bonewald LF (2011) Cell Line IDG-SW3 Replicates Osteoblast-to-Late-Osteocyte Differentiation In Vitro and Accelerates Bone Formation In Vivo. Journal of Bone and Mineral Research 26(11):2634–2646 [PubMed: 21735478]
59. Bullock WA, Hoggatt AM, Horan DJ, Lewis KJ, Yokota H, Hann S,… Robling AG (2019) Expression of a Degradation-Resistant beta-Catenin Mutant in Osteocytes Protects the Skeleton From Mechanodeprivation-Induced Bone Wasting. J Bone Miner Res 34(10):1964–1975. [PubMed: 31173667]

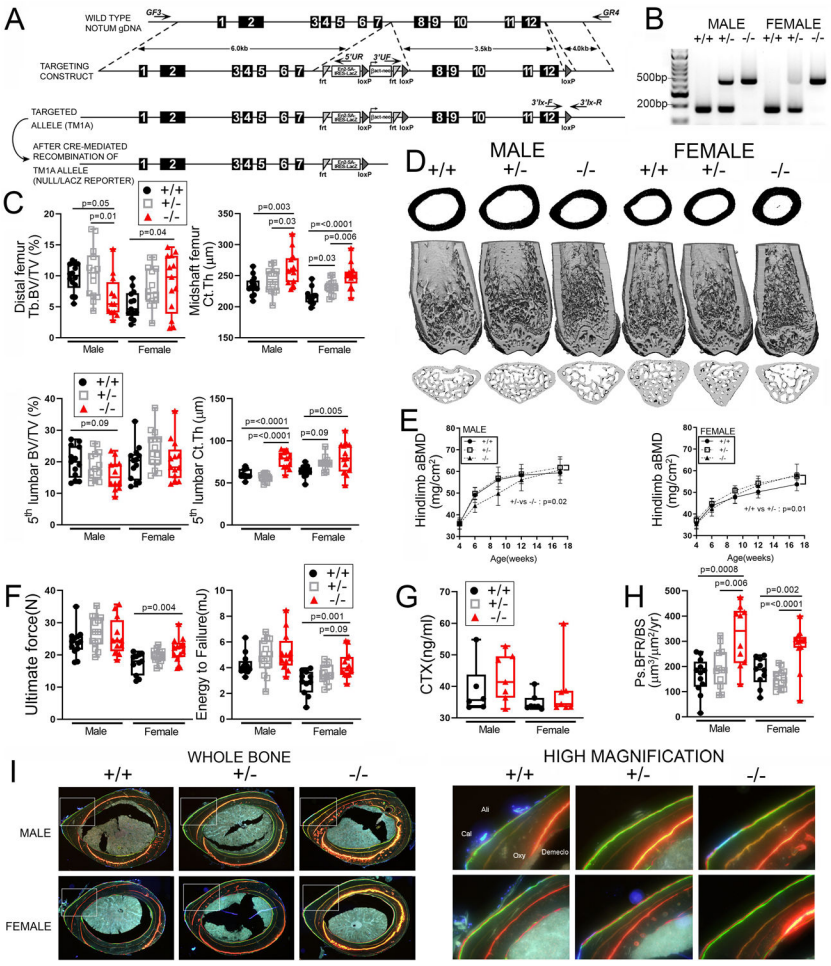

Figure 1. Generation and characterization of *Notum* global knock out mice model.

(A) Schematic representation of the targeting strategy for *Notum* global knock out alleles. A *LacZ* reporter cassette and *Neo*^{R} selection cassette were inserted into intron 7 along with *loxP* and *frt* sites as shown. Successfully targeted mice were bred to germline Cre-expressing mice (EIIa-Cre) to generate a Notum knockout/LacZ-knockin allele. **(B)** Agarose PCR gel showing successful detection of the mutant (190bp) and WT (~500bp) alleles from mouse DNA extracted from tail clips. **(C)** μCT-derived trabecular bone volume fraction (Tb.BV/TV) at the distal femur and 5th lumbar vertebra (left column), and cortical thickness (Ct.Th) at the midshaft femur and 5th lumbar vertebra (right column) collected from 17-wk-old male and female mice. **(D)** Representative midshaft femur (upper row), distal femur (middle row) and lumbar vertebra (lower row) μCT reconstructions from 17-wk-old male and female mice. **(E)** Serial measurements of the areal bone mineral density (aBMD) derived from dual-energy X-ray absorptiometry (DXA) scans in WT, heterozygous, and homozygous knockout mice from 4–17 wks of age. **(F)** Biomechanical properties (ultimate force and energy to failure) measured by 3-point-bending test on whole femora collected from 17-wk-old mice. **(G)** CTX (C-telopeptide) levels in serum from 6-week-old male and female mice. **(H)** Periosteal bone formation rate per unit bone surface (BFR/BS) measured using the tetracycline label (9 wks) and calcein label (16 wks). Mice were sacrificed at 17

wks. **(I)** Representative fluorochrome-labeled midshaft femur histologic cross-sections. The white box in the top row is magnified in the bottom panels to visualize bone formation between labels. Portions of an earlier (4 wks) demeclocycline label and a final (16.7 wks) alizarin label are visible but were not used for measurements. Orange = demeclocycline; gold = oxytetracycline, green = calcein; red = alizarin complexone, respectively. Error bars shown in ± S.D. in DEXA graphs (to facilitate visibility of the error). Panel C,F:n=11–14 mice/group. Panel E: n=12–14 mice/group. Panel G: n=6–7 mice/group. Panel H: n=10–14 mice/group. Panel E was analyzed using repeated-measures one-way ANOVA followed by Tukey-post hoc tests. Panel G was analyzed using student's t-test. Other panels were analyzed using One-way ANOVA followed by Tukey-post hoc tests.

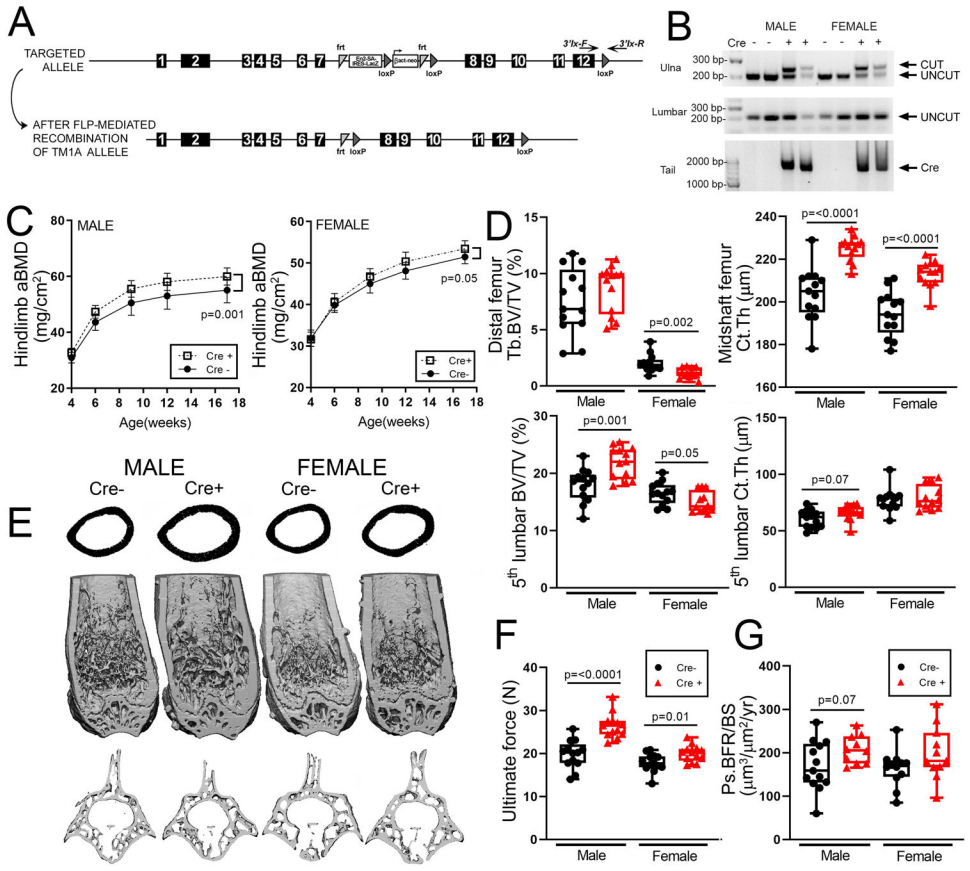

Figure 2. Generation of a Notum loss-of-function floxed allele and conditional deletion in Prx1-expressing cells.

(A) Schematic representation of the *Notum* floxed allele, generated from the tm1a targeted mice. tm1a mice were crossed to Rosa26-Flp mice to recombine and delete the LacZ/NeoR cassettes plus the 5' loxP site, leaving a lonely frt site and exons 8–12 flanked by a pair of loxP sites. These mice were subsequently bred to Prx1-Cre transgenics to induce limb-bud mesenchymal deletion of Notum. **(B)** Agarose PCR gel showing (upper gel) recombination of the floxed allele in the ulnar cortex among Cre-positive but not -negative mice, (middle gel) lack of recombination in the vertebral bone (axial skeleton) regardless of Cre status, and (lower gel) presence of the Prx1-Cre transgene assayed from tail snips. The same 8 mice are shown in each gel. **(C)** Serial aBMD measurements from DXA scans collected intermittently from 4–17 wks. **(D)** μCT-derived trabecular bone volume fraction (Tb.BV/TV) at the distal femur and 5th lumbar vertebra (left column), and cortical thickness (Ct.Th) at the midshaft femur and 5th lumbar vertebra (right column) collected from 17-wk-old male and female mice. **(E)** Representative midshaft femur (upper row), distal femur (middle row) and lumbar vertebra (lower row) μCT reconstructions from 17-wk-old male and female mice. **(F)** Ultimate force measured by 3-point-bending test on whole femora collected from 17-wk-old mice. **(G)** Periosteal bone formation rate per unit bone surface (BFR/BS) measured using the tetracycline label (9 wks) and calcein label (16 wks). Error bars shown in ± S.D. in DEXA graphs (to facilitate visibility of the error). Panel C: n=13 mice/group. Panel D: n=12–13 mice/group. Panel F : n=13 mice/group. Panel G: n=10–13 mice/group.

Panel C was analyzed using repeated-measures ANOVA. Other panels were analyzed using student's t-test.

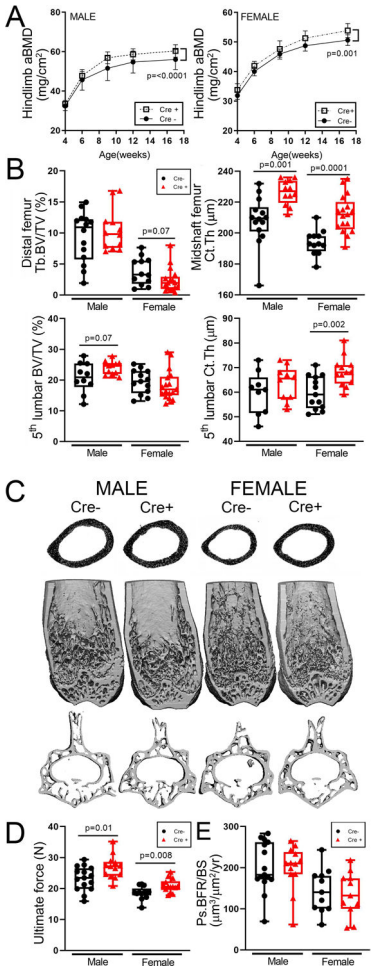

Figure 3. Conditional deletion of Notum from Dmp1-expressing cells

(A) Serial aBMD measurements from DXA scans collected intermittently from 4–17 wks. **(B)** μCT-derived trabecular bone volume fraction (Tb.BV/TV) at the distal femur and 5th lumbar vertebra (left column), and cortical thickness (Ct.Th) at the midshaft femur and 5th lumbar vertebra (right column) collected from 17-wk-old male and female mice. **(C)** Representative midshaft femur (upper row), distal femur (middle row) and lumbar vertebra (lower row) μCT reconstructions from 17-wk-old male and female mice. **(D)** Ultimate force measured by 3-point-bending test on whole femora collected from 17-wk-old mice. **(E)** Periosteal bone formation rate per unit bone surface (BFR/BS) measured using the tetracycline label (9 wks) and calcein label (16 wks). Error bars shown in ± S.D. in DEXA graphs (to facilitate visibility of the error). Panel A: n=13–16 mice/group Panel B: n=9–17 mice/group. Panel D: n=13–15 mice/group. Panel E: n=11–15 mice/group. Panel A was analyzed using repeated-measures ANOVA. Other panels were analyzed using student's t-test.

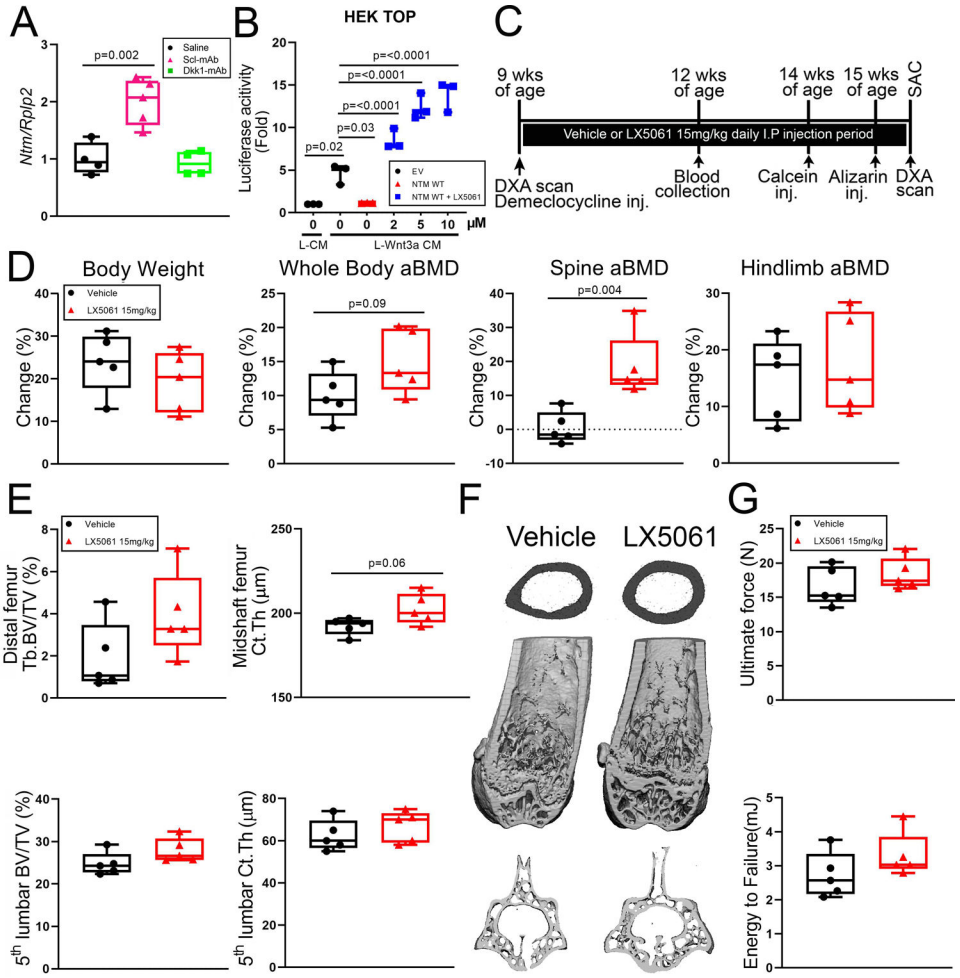

Figure 4. The *Notum* small molecule inhibitor LX5061 marginally improves cortical bone.

(A) Relative expression levels of *Notum* in the femur and tibial cortex from WT mice, 48 hrs after single treatment with vehicle, sclerostin antibody (*Scl-mAb*), or Dkk1 antibody (*Dkk1-mAb*) at 25mg/kg. **(B)** Luciferase activity measured in the Wnt/β-catenin reporter cell line HEK-Topflash treated with Wnt3a conditioned medium (Wnt3a-CM) or control medium (L-CM), after transfection with empty vector (EV) or Notum WT (NTM WT) expression plasmids, with different concentrations of the small molecule Notum inhibitor LX5061. Luciferase activity was measured after 24 hours after treatment. **(C)** Experimental design and timeline indicating DXA scans, fluorochrome labeling, blood collection, and LX5061 treatment duration. **(D)** Percent change in body weight and DXA-derived whole body, spine, and hindlimb areal bone mineral density (aBMD), calculated using the beginning (9 wks) and final (16 wks) scans. **(E)** μCT-derived trabecular bone volume fraction (Tb.BV/TV) at the distal femur and 5th lumbar vertebra (left column), and cortical thickness (Ct.Th) at the midshaft femur and 5th lumbar vertebra (right column) collected from 16-wk-old female mice. **(F)** Representative midshaft femur (upper row), distal femur (middle row) and lumbar vertebra (lower row) μCT reconstructions from 16-wk-old female mice treated with LX5061 or vehicle. **(G)** Biomechanical properties (ultimate force and energy to failure) measured by 3-point-bending test on whole femora collected from 16-wk-old mice treated with LX5061

or vehicle. Luciferase assays were conducted in 3 independent experiments performed in triplicate and similar results were obtained. Panel A: n=4–5 mice /group. Panel D–G: n=5 mice /group. Panel A, B were analyzed using One-way ANOVA followed by Tukey-post hoc tests. Other panels were analyzed using student's t-test.

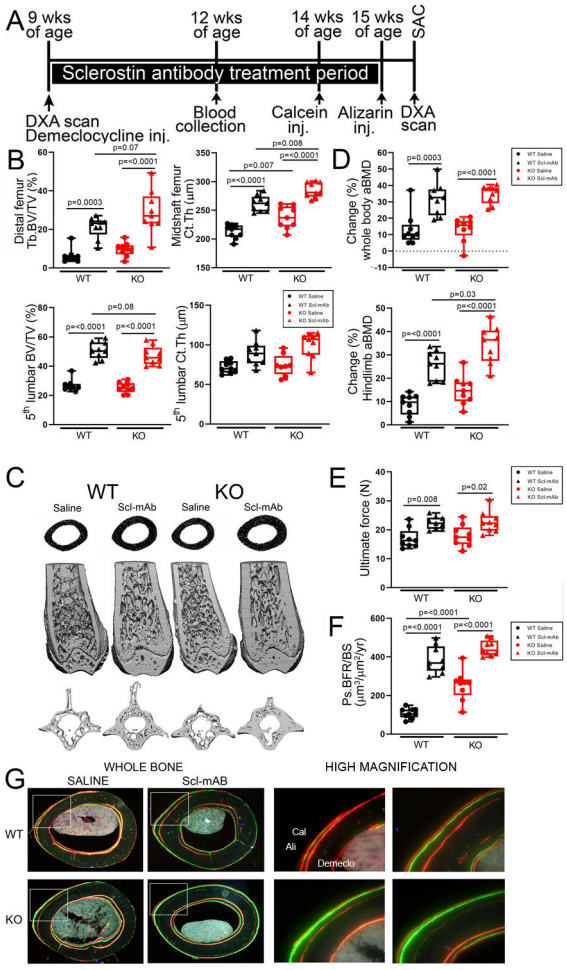

Figure 5. Sclerostin inhibition on a *Notum*-null background has additive effects on increasing cortical bone formation.

(A) Experimental design and timeline indicating DXA scans, fluorochrome labeling, blood collection, and sclerostin antibody (Scl-mAb) treatment duration. **(B)** μCT-derived trabecular bone volume fraction (Tb.BV/TV) at the distal femur and 5th lumbar vertebra (left column), and cortical thickness (Ct.Th) at the midshaft femur and 5th lumbar vertebra (right column) collected from 16-wk-old female mice. **(C)** Representative midshaft femur (upper row), distal femur (middle row) and lumbar vertebra (lower row) μCT reconstructions from 16-wk-old WT or Notum $^{-/-}$ (KO) female mice treated with Scl-mAb or vehicle. **(D)** Percent change in DXA-derived whole body and hindlimb areal bone mineral density (BMD), calculated using the beginning (9 wks) and final (16 wks) scans. **(E)** Ultimate force measured by 3-point-bending test on whole femora collected from 16-wk-old mice. **(F)** Periosteal bone formation rate per unit bone surface (BFR/BS) measured using the demeclocycline (9 wks) and calcein (14 wks) labels. **(G)** Representative fluorochrome-labeled midshaft femur histologic cross-sections. The white box in the left panel is magnified in the right panel to visualize bone formation between labels. A final (15 wks) alizarin label is visible but was not used for measurements. Orange = demeclocycline; green = calcein; red = alizarin complexone, respectively. Panel B: n=8–9 mice/group. Panel D–F:

n=9 mice/group. All panels were analyzed using two-way ANOVA followed by Tukey-post hoc tests.

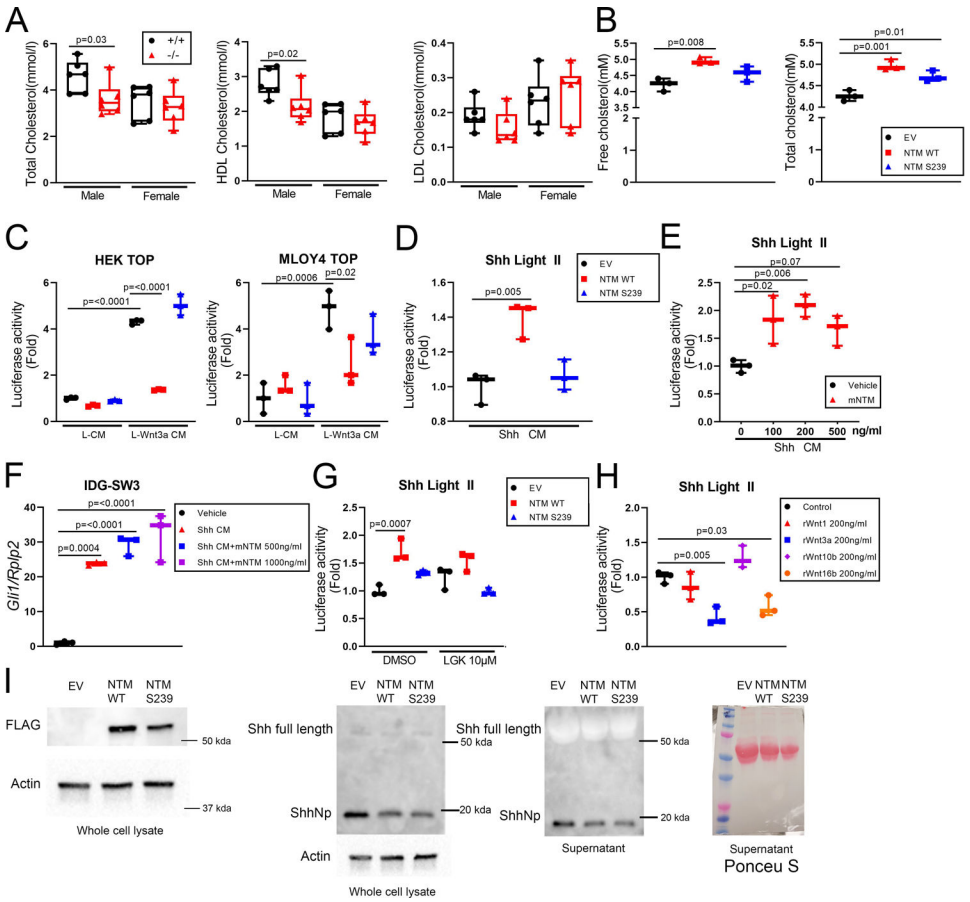

Figure 6. *Notum* exhibits distinct activity in Wnt and Shh signaling pathways.

(A) Serum levels of total (left panel) high density lipoprotein (middle panel) and low density lipoprotein (right panel) cholesterol measured in the serum of 17-wk-old male and female Notum WT (+/+) and global knockout (−/−) mice. **(B)** Free (left panel) and total (right panel) cholesterol concentration in the culture media of ECR Shh cells (stably transfected to produce large amounts of Shh) 48 hrs after transient transfection with empty vector (EV), Notum WT (NTM WT) or mutant Notum (NTM S239) that harbors a point mutation at residue 239 (functionally dead for Wnt lipase activity). **(C)** Luciferase activity measured in 2 different Wnt/β-catenin reporter cell lines, HEK-Topflash (left panel) and MLOY4-Topflash (right panel) that were transiently transfected with EV, NTM, or NTM-S239 and treated with Wnt3a conditioned medium (L-Wnt3a CM) or control medium (L-CM). Luciferase was measured 24 hrs after treatment with conditioned medium. **(D)** Luciferase activity measured in the Shh/Gli reporter cell line Light II, that were transiently transfected with EV, NTM, or NTM-S239 and treated with Shh conditioned medium (Shh CM). Luciferase was measured 24 hrs after treatment with conditioned medium. **(E)** Luciferase activity measured in Light II cells treated with Shh conditioned media and different doses of recombinant mouse Notum protein (mNTM). Luciferase was measured 24 hrs after treatment with conditioned medium. **(F)** Gli1 mRNA expression in IDG-SW3 osteocytic cells after treatment with Shh CM with or without recombinant mouse Notum at two different concentrations. **(G)** Luciferase activity in Light II cells that were transfected with EV, NTM, or NTM WT plasmids, then

pretreated with vehicle (DMSO) or the porcupine inhibitor LGK974 for 24 hrs prior to exposure to Shh CM. **(H)** Luciferase activity measured in Light II cells treated with different recombinant Wnts for 24 hrs. **(I)** Western blots and Ponceau (far right) of whole cell lysate and supernatant from ECR Shh cells 48 hrs after transfection with indicated plasmids. All experiments were conducted in 3–4 independent experiments, performed in triplicates and similar results were obtained. Panel A: n=6 mice/group. Panel A, B were analyzed using student's t-test. Panel F was analyzed using two-way ANOVA followed by Tukey-post hoc tests. Other panels were analyzed using one-way ANOVA followed by Tukey-post hoc tests.

Table 1.

qPCR primer information

qPCR primers	Forward	Reverse
Notum(NTM)	GATGGTCCCAGAGCGTTG	TACCACGAACACCGGACAG
LacZ	TTTCAGCCGCGCTGTACT	CGTAGGTAGTCACGCAACTCG
Mastermix	Catalog #	
Sclerostin(Sost)	Mm 00470479	
RPLP2	Mm 03059047	
GAPDH	Mm 99999915	